ELSEVIER

Journal of Nuclear Materials 274 (1999) 15–22

journal of nuclear materials

www.elsevier.nl/locate/jnucmat

Thermophysical properties of rock-like oxide fuel with spinel–yttria stabilized zirconia system

N. Nitani [a,*], T. Yamashita [a], T. Matsuda [b], S.-i. Kobayashi [b], T. Ohmichi [c]

[a] *Japan Atomic Energy Research Institute, Tokai, Ibaraki 319-1195, Japan*
[b] *Nuclear Fuel Industries Ltd., Kumatori, Osaka, 590-0451, Japan*
[c] *Research Organization for Information Science and Technology, Tokai, Ibaraki, 319-1195, Japan*

Abstract

Thermal expansion, thermal diffusivity, melting temperature, Vickers hardness and creep rate of the rock-like oxide (ROX) fuel were measured with the $MgAl_2O_4$(spinel)–ZrO_2(Y,Gd) (YSZ: stabilized zirconia) system and the $MgAl_2O_4$–YSZ–UO_2 system in the temperature range between room temperature and 1800 K in order to evaluate thermophysical properties. Thermal expansion coefficients of $MgAl_2O_4$–YSZ composites increased with increasing YSZ content and the values were well represented by the Turner's equation. Addition of UO_2 to $MgAl_2O_4$–YSZ composite resulted in an increase of thermal expansion. Thermal conductivity values of the $MgAl_2O_4$–YSZ composites decreased with increasing YSZ content and agreed with predictions of the Maxwell–Eucken equation. The eutectic temperature of $MgAl_2O_4$–YSZ and $MgAl_2O_4$–YSZ–UO_2 systems was found to be 2200 K. High temperature hardness of the composites was higher than that of YSZ or $MgAl_2O_4$. The hardness of ROX fuel was considerably higher than that of UO_2. The creep rate of $MgAl_2O_4$–YSZ composite was controlled by the lattice diffusion of YSZ.

1. Introduction

Regarding the annihilation of plutonium, we have proposed plutonium rock-like oxide (ROX) fuels [1]. The fuel design applies to a Pu once-through burning system combined with direct disposal of spent fuels after cooling. The ROX fuel is a multi-phase composite of nuclear stable mineral-like (rock-like) compounds such as ZrO_2, Al_2O_3, $MgAl_2O_4$ and so on, and plutonium is expected to solidify in a fluorite phase.

YSZ–Al_2O_3–$MgAl_2O_4$ system was selected as a candidate for ROX fuel, and phase relations, acid resistances and irradiation stabilities have been studied [1–5]. From the view point of irradiation stability, $MgAl_2O_4$ is preferable to Al_2O_3. The fuel in $MgAl_2O_4$–YSZ composite form appears to be the favorite form for the ROX fuel [5,6]. Little is known about the thermophysical properties of $MgAl_2O_4$–YSZ composite, so it is essential to measure the physical properties needed to predict the in-pile behavior of the ROX fuel. In this study, thermophysical and mechanical properties of a $MgAl_2O_4$–YSZ composite such as thermal expansion, thermal diffusivity, melting temperature, high temperature hardness and creep rate were measured and evaluated. Composites containing UO_2 were also evaluated, using uranium as a stand-in for plutonium.

2. Experimental

2.1. Sample preparation and characterization

An acid solution of the YSZ components was prepared by dissolving Y_2O_3, Gd_2O_3 and $ZrO(NO_3)_2{\cdot}2H_2O$ into a dilute HNO_3 solution. The YSZ had a composition of 88.8 mol% ZrO_2 + 11.0 mol% Y_2O_3 + 0.2 mol% Gd_2O_3. Solutions with Mg, Al and U were also prepared by adding MgO, $Al(NO_3)_3{\cdot}9H_2O$ and $UO_2(NO_3)_2{\cdot}6H_2O$, respectively, to the original dilute HNO_3 solution. The solutions were prepared by mixing standard acid solutions in the composition shown in Table 1. The mixed

* Corresponding author: Fax: +81-29 282 5935; e-mail: nitani@analchem.tokai.jaeri.go.jp

0022-3115/99/$ – see front matter
PII: S0022-3115(99)00077-X

Table 1
Composition of samples (mol%)

Sample No.	$MgAl_2O_4$	YSZ	UO_2
1	100.0	0.0	0.0
2	64.3	35.7	0.0
3	40.3	59.7	0.0
4	10.1	89.9	0.0
5	0.0	100.0	0.0
12	54.5	30.3	15.2
13	35.0	52.0	13.0

solutions were evaporated at 400 K, and the residues were calcined at 1100 K. Pellets were pressed from the calcined powder and sintered at 2050 K for 4 h in the stream of 75% H_2 / 25% N_2.

Sample No. 1 was the single phase of $MgAl_2O_4$, No. 2–4 were the composites of YSZ and $MgAl_2O_4$, and No. 5 was a single phase of YSZ. Sample No. 12 and No. 13 were prepared by adding UO_2 to No. 2 and No. 3, respectively. The UO_2 content was 15.2 mol% for No. 12, and 13.0 mol% for No. 13.

Microstructures, phase relations and distributions of elements in samples were examined by scanning electron micro-analysis (SEM), X-ray diffraction and electron probe micro-analysis (EPMA). The SEM images of the sintered composites are shown in Fig. 1. All samples show a homogeneous distribution of grains with no cracking. Grain size was less than 10 μm. It was confirmed that the uranium dioxide was dissolved in the fluorite-type phase by X-ray diffraction and EPMA.

The densities were measured by a He gas pycnometry method on the powder samples, and the bulk densities of pellets were calculated from mass and dimension measurements, which were used for the determination of porosity and the volume fractions of each phase. The density, porosity and volume fraction values of each phase are shown in Tables 2 and 3.

2.2. Thermophysical property measurements

The following measurements were carried out in the temperature range from room temperature to 1800 K. Samples used were approximately 9 mm in diameter and

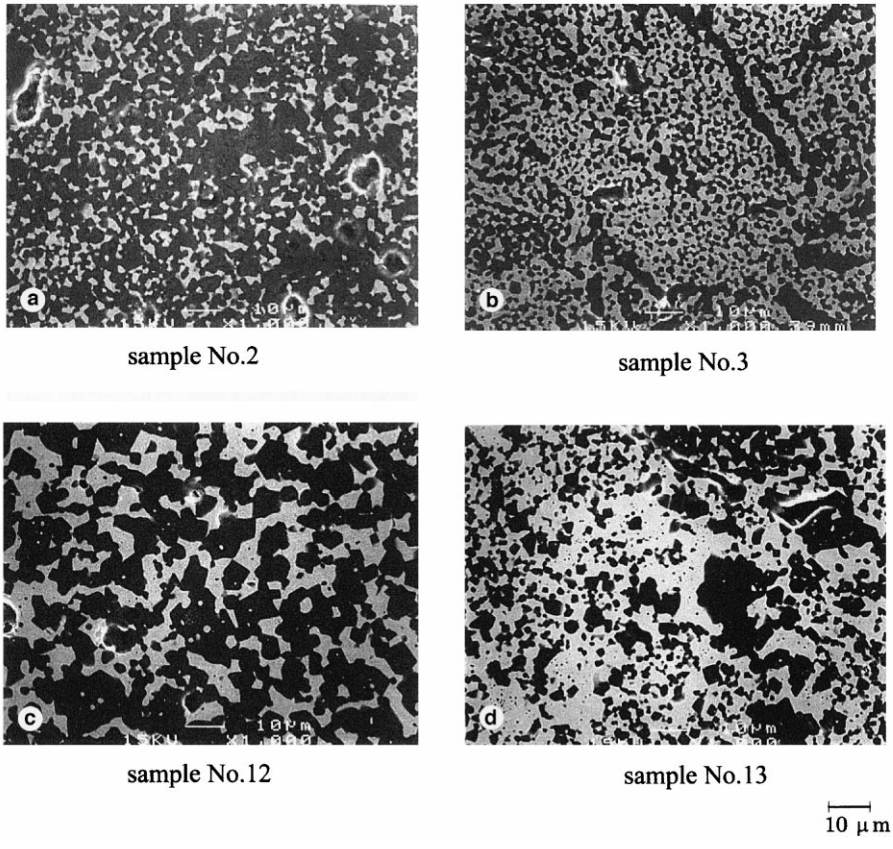

Fig. 1. SEM images of samples. Samples No. 2 and No. 3 are composites of the $MgAl_2O_4$–YSZ system and No. 12 and No. 13 are composites of the $MgAl_2O_4$–YSZ–UO_2 system. The bright regions are the fluorite-type phase, and the dark regions are $MgAl_2O_4$.

Table 2
Density and porosity of sintered compacts

Sample No.	Density (g cm^{-3})	Bulk density (g cm^{-3})	Porosity (%TD)
1	3.52	3.21	8.9
2	4.09	3.95	3.4
3	4.60	4.47	2.7
4	5.49	5.12	6.7
5	5.89	5.19	11.9
12	4.91	4.74	3.4
13	5.37	5.06	5.7

Table 3
Volume fraction of samples

Sample No.	Volume fraction (%)		
	$MgAl_2O_4$	YSZ	UO_2
1	100.0	0.0	0.0
2	77.5	22.5	0.0
3	56.4	43.6	0.0
4	17.7	82.3	0.0
5	0.0	100.0	0.0
12	68.5	19.9	11.6
13	50.0	38.7	11.3

10 mm in height. Thermal expansion was measured by the dilatometric method in a reducing atmosphere. Sapphire was used as the standard. Measurements were carried out at progressively increasing temperature. Thermal diffusivity was measured by the laser flash method with disk samples of approximately 2 mm thickness. Observed values were corrected for the effects of thermal expansion. The melting temperature was determined by thermal arrest at gradually increasing temperature. The sample of approximately 10 mg was heated on tungsten in an argon atmosphere. Al_2O_3, Y_2O_3 and HfO_2 standards were used for temperature calibration. Vickers hardness was measured by conventional methods. Creep tests were carried out under constant compressive stress in vacuum. The steady-state creep rate was calculated from the time–strain curve.

3. Results and discussion

3.1. Thermal expansion

The thermal expansion of samples No. 1–5 is shown in Fig. 2(a) together with UO_2 data [7] for comparison. The thermal expansions of all the samples used in this work are lower than that of UO_2. Thermal expansion increases with YSZ content, which qualitatively agrees with the fact that thermal expansion of YSZ is larger than that of $MgAl_2O_4$.

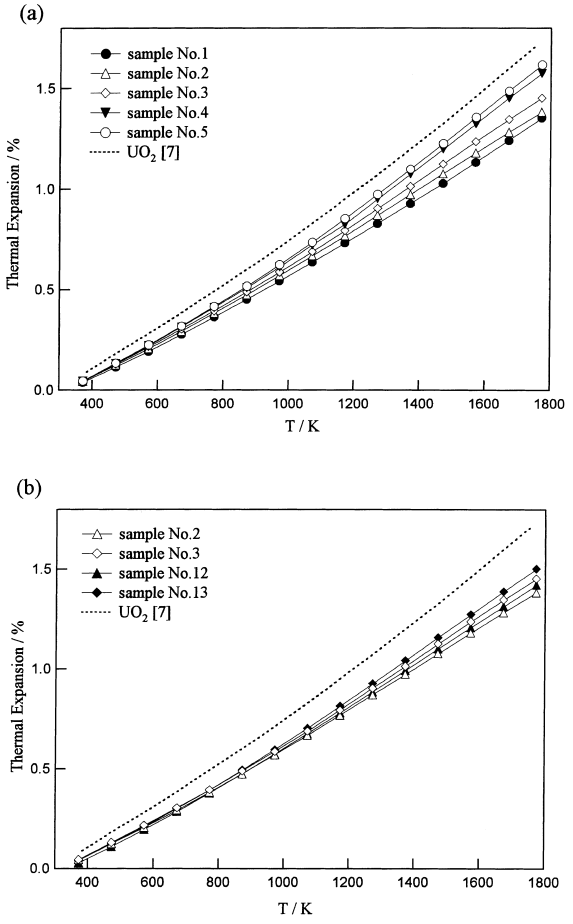

Fig. 2. Thermal expansion of (a) YSZ–$MgAl_2O_4$ system and (b) $MgAl_2O_4$–YSZ–UO_2 system. Dotted line is the data of UO_2 [7].

The measured thermal expansion coefficient, α, of $MgAl_2O_4$–YSZ composites can be compared with that calculated using the following equations:

$$\alpha = \sum_i \phi_i \cdot \alpha_i, \tag{1}$$

$$\alpha = \frac{\sum \alpha_i \cdot K_i \cdot w_i \cdot \rho_i^{-1}}{\sum K_i \cdot w_i \cdot \rho_i^{-1}}, \tag{2}$$

where ϕ_i is volume fraction of component i, K_i is its bulk modulus, w_i is its weight fraction and ρ_i is its density. Eq. (2) is known as Turner's equation [8].

Results are shown in Fig. 3 together with observed values. Turner's equation can represent observed values more accurately than Eq. (1). The difference between the observed and calculated values was less than 2%.

The thermal expansions of the UO_2 containing systems are shown in Fig. 2(b). The thermal expansion of UO_2 containing systems is slightly higher than those of samples containing no UO_2. This shows that the

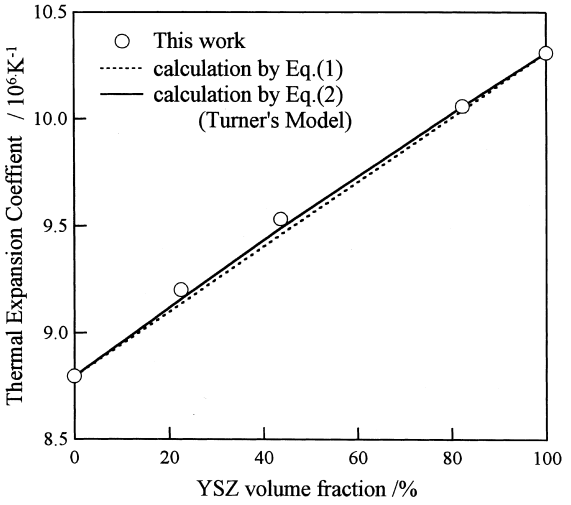

Fig. 3. Estimation of thermal expansion coefficient of composite. Dotted line is calculation by Eq. (1) and solid line is calculation by Turner's equation.

addition of UO_2 results in an increase of the volume fraction of the fluorite-type phase, and an increase in the thermal expansion of the fluorite phase since UO_2 has a higher thermal expansion than YSZ.

3.2. Thermal conductivity

Thermal conductivity data were obtained from data of thermal diffusivity, specific heat and density of the samples. The specific heat of each sample was calculated by the additive law, using data from literature on each oxide [9]. Thermal conductivity of the samples with 95%TD was calculated from observed value using Loeb's improved equation, as follows:

$$\kappa = \kappa_0 \cdot (1 - 2.5 \cdot P), \tag{3}$$

where κ is thermal conductivity of the sample with porosity P and κ_0 is thermal conductivity of the sample with 100%TD. The corrected thermal conductivity of sample No. 1 ($MgAl_2O_4$) showed good agreement with the literature data [10].

The thermal conductivities of samples No. 1–5 are shown in Fig. 4(a) with UO_2 data [7]. The thermal conductivities of samples No. 1 and No. 2 are higher than that of UO_2 for temperatures ranging from room temperature to 1700 K, and that of sample No. 3 is higher than that of UO_2 above 700 K. The thermal conductivity of the composites increases with $MgAl_2O_4$ content. The thermal conductivity of sample No. 4 shows a similar temperature dependence to that of YSZ, which is related to the high volume fraction of YSZ (82 vol.%).

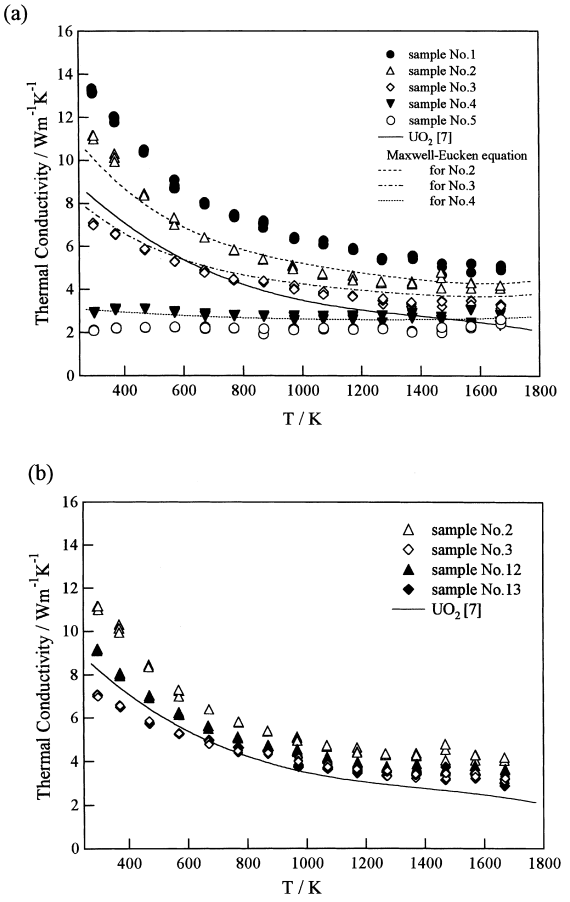

Fig. 4. Thermal conductivity of samples. (a) Thermal conductivity of YSZ–$MgAl_2O_4$ system and calculations by Maxwell–Eucken equations. (b) Thermal conductivity of $MgAl_2O_4$–YSZ–UO_2 system. Solid line is data of UO_2 [7].

The thermal conductivity of the composites was calculated from the thermal conductivities of the pure phases using the Maxwell–Eucken equation [11],

$$\kappa = \kappa_1 \cdot \left(\frac{2 \cdot \kappa_1 + \kappa_2 - 2 \cdot \phi_2 \cdot (\kappa_1 - \kappa_2)}{2 \cdot \kappa_1 + \kappa_2 + \phi_2 \cdot (\kappa_1 - \kappa_2)} \right]. \tag{4}$$

This model assumes the composite to be a mixture of matrix and dispersed particles.

Calculated results are shown in Fig. 4(a). They agree within 5% for observed values of samples No. 2 and No. 4, and within 10% for observed values of sample No. 3 above 500 K. The agreement between the calculated and the observed values of sample No. 3 is not as good as those of No. 2 and No. 4. Since the volume fraction of YSZ is close to that of $MgAl_2O_4$, it is difficult to estimate the value by the particle dispersion model.

The thermal conductivities of the UO_2 containing system are shown in Fig. 4(b). The thermal conductivity of sample No. 12 is higher than that of UO_2 in the

temperature range between room temperature and 1700 K, and the value is approximately 30% higher at 1500 K. Above 700 K, the thermal conductivity of sample No. 13 is higher than that of UO_2. Sample No. 12 shows lower thermal conductivity than sample No. 2, because the adding of UO_2 resulted in an increase in volume fraction of the fluorite-type phase from 22% to 30%. Sample No. 13 with a high volume fraction of the fluorite-type phase showed lower thermal conductivity than that of sample No. 12. The thermal conductivity of sample No. 13 is similar to that of sample No. 3, because the volume fractions of the fluorite phase of these composites are almost identical.

3.3. Melting temperature

The measured melting temperatures are summarized in Table 4. The melting temperature of the YSZ is 2996 K which is very close to that of ZrO_2 [9]. It is found that the addition of Y_2O_3 and Gd_2O_3 to ZrO_2 does not influence significantly the melting temperature of ZrO_2. The eutectic temperature of the $MgAl_2O_4$–YSZ system was determined to be 2200 K from the results of samples No. 2–4. The melting temperature of the UO_2 containing system was almost identical to that of the UO_2-free system.

The SEM observation of the samples after melting tests revealed that sample No. 2 consisted of $MgAl_2O_4$ and the eutectic, and samples No. 3 and No. 4 consisted of the fluorite-type phase and the eutectic (Fig. 5). Since the amount of the fluorite-type phase in sample No. 3 was low, it appears that the eutectic composition of the $MgAl_2O_4$–YSZ system exists more to the $MgAl_2O_4$ side compared to the composition of No. 3.

The phase diagram of the $MgAl_2O_4$–YSZ pseudo-binary system was calculated using an ideal solution model. Assuming that the system is a single eutectic, the eutectic temperature and composition can be inferred from the junction of the two liquidus curves. The mole fraction of solvent phase at the liquidus (x) is given by

$$\ln x = \frac{\Delta H_{\mathrm{fus}}}{R} \cdot \left(\frac{1}{T_{\mathrm{m}}} - \frac{1}{T} \right), \tag{5}$$

Table 4
Melting temperature of samples

Sample No.	Melting temperature (K)
1	2375.0
2	2203.7
3	2201.6
5	2996.6
12	2206.2
13	2205.6

where ΔH_{fus} is heat of fusion and T_{m} is melting temperature of the component. The heat of fusion of ZrO_2 was used in the calculation because that of YSZ was not available [9]. It was also assumed that the heat of fusion was constant in this temperature range.

The result of calculation is shown as dotted lines in Fig. 6. The calculated melting temperature is about 100 K higher than the experimental value. The calculated eutectic composition is 37 mol% YSZ which is similar to the composition of sample No. 2. This differs from the experimental result; the eutectic point exists near the composition of sample No. 3. The difference between the calculated and observed eutectic points can be attributed to the various assumptions involved. (1) The solutions may not be ideal, when some interaction/association occur in the liquids, as ΔG_{liq} of the associated solution becomes smaller than that of the ideal solution. (2) The heat of fusion of YSZ is different from that of ZrO_2, the former is expected to be smaller. The decrease of ΔG_{liq} and/or ΔH_{fus} causes the decrease of the eutectic temperature and shift of the eutectic composition to the YSZ side.

The after melting test sample No. 13 also consisted of the fluorite-type and the eutectic phases, similar to that observed for UO_2-free system. The distribution of the elements of Zr and U in sample No. 13 was observed by EPMA. Uranium and zirconium show similar distributions in both the fluorite and eutectic phases. It was confirmed that around the melting temperature the two-phase separation of the fluorite type phase does not occur.

3.4. High temperature hardness

The Vickers hardnesses of samples No. 1–3 and No. 5 are shown in Fig. 7. The hardness values of samples No. 2 and No. 3 are larger than those of samples No. 1 and No. 5 which are the pure phase components of the composites. It is considered that the porosity of the composites are lower than those of the components (see Table 2).

In the composite systems, hardness increases with $MgAl_2O_4$ content. The hardness of sample No. 12 is almost equivalent to that of sample No. 3. The Vickers hardness of UO_2 was about 2 GPa at 700 K [12]. The hardness of the ROX fuel is considerably higher than that of the UO_2. Though it is not possible to relate the value of the hardness to the value of the elastic constant and mechanical strength directly, the hardness can be regarded as a scale of the mechanical strength of the sample.

3.5. Creep rate

The stress dependency of creep rate is shown in Fig. 8. The creep rate of sample No. 2 is smaller than

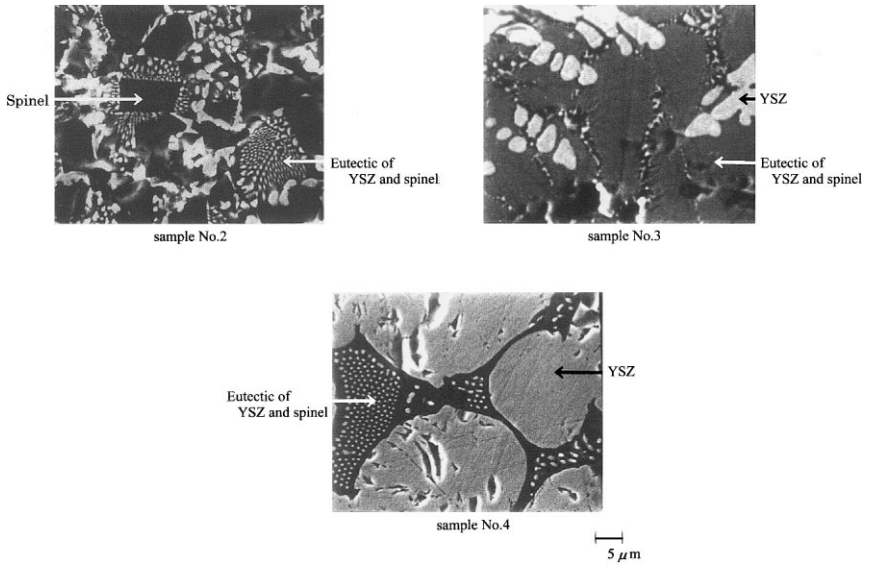

Fig. 5. SEM images of composites after melting test.

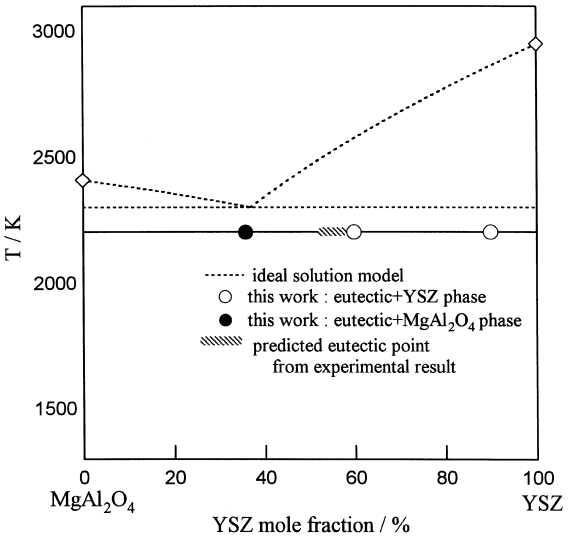

Fig. 6. Calculated phase diagram of pseudo-binary $MgAl_2O_4$–YSZ system. Dotted line is the calculated result by ideal solution model.

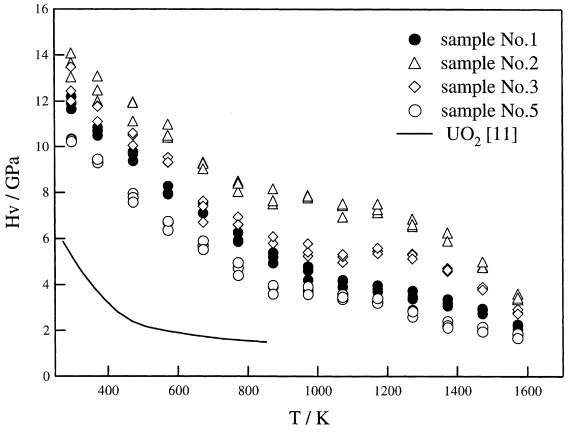

Fig. 7. Vickers hardness of ROX fuel. Solid line is data of UO_2 [12].

that of sample No. 3, which qualitatively agrees with the result of the hardness tests described above. The stress indices of samples No. 2 and No. 3 are approximately 1 and 2, respectively. This fact indicates that the creep mechanism of sample No. 2 is probably diffusional creep for the tested conditions. The creep mechanism of sample No. 3 may be partly diffusional creep, and partly dislocation creep. Diffusional creep rates are given by

$$\dot{\varepsilon} = A \cdot \left(\frac{\sigma}{d^p}\right) \cdot \exp\left(\frac{-\Delta H}{RT}\right), \tag{6}$$

where σ is stress, d is grain size, p is grain size index, ΔH is activation energy, and A is a constant.

The temperature dependency of the creep rate is shown in Fig. 9. In this temperature range, a linear relationship between $\ln \dot{\varepsilon}$ and T^{-1} was observed and the activation energy was calculated for each sample.

The activation energies of samples No. 2 and No. 3 are 572 and 616 kJ mol^{-1}, respectively. The activation energy of lattice diffusion of yttria doped ZrO_2 is

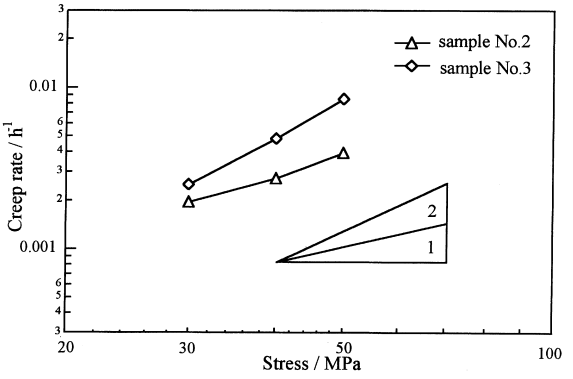

Fig. 8. Stress dependency of creep rate of ROX fuel.

550 ± 70 kJ mol^{-1} [13], and that of boundary diffusion is approximately 500 kJ mol^{-1} [14]. The activation energy of lattice diffusion of the $MgAl_2O_4$ is 440 kJ mol^{-1} [15]. Since the observed activation energies of the composites are close to that of lattice diffusion in yttria doped ZrO_2, the creep of composite samples No. 2 and No. 3 is considered to be limited by the lattice diffusion of YSZ.

4. Conclusion

The thermophysical properties such as thermal expansion, thermal diffusivity, melting temperature, Vickers hardness and creep rate were measured and evaluated for ROX fuel with the $MgAl_2O_4$–YSZ and the $MgAl_2O_4$–YSZ–UO_2 systems. The following observations were made:

(1) Thermal expansion of the $MgAl_2O_4$–YSZ composites increases with increasing YSZ content. Turner's equation represented observed values within an error of 2%. The thermal expansion of the rock-like fuel is 10–15% lower than that of UO_2.

(2) Thermal conductivity increases with the $MgAl_2O_4$ content. The thermal conductivity of sample No. 12 which is the most hopeful composition for ROX fuel is higher than that of UO_2 in the temperature range from room temperature to 1700 K. Thermal conductivity of the $MgAl_2O_4$–YSZ composite is well represented by the Maxwell–Eucken equation.

(3) The melting temperature of the $MgAl_2O_4$–YSZ system is found to be 2200 K. Addition of UO_2 to the $MgAl_2O_4$–YSZ system does not affect the melting temperature very much.

(4) The high temperature hardness of the composites is larger than that of the pure-phase components. The hardness of ROX fuel is considerably higher than that of the UO_2. In the composite system, the hardness increases with increasing $MgAl_2O_4$ content.

(5) The creep rate decreases with increasing $MgAl_2O_4$ content. The creep of the $MgAl_2O_4$–YSZ composite is limited by the lattice diffusion of YSZ.

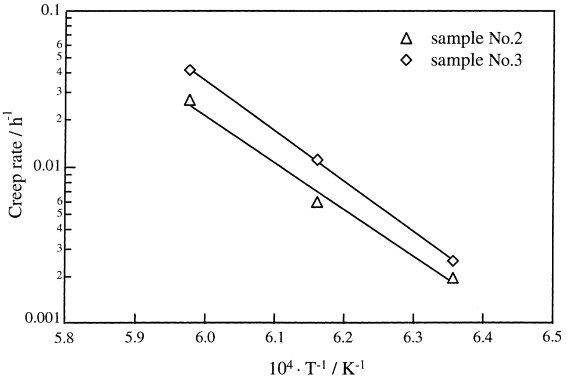

Fig. 9. Temperature dependency of creep rate of ROX fuel.

References

[1] H. Akie, T. Muromura, H. Takano, S. Matsuura, Nucl. Technol. 107 (1994) 189.
[2] H. Akie, H. Takano, T. Muromura, N. Nitani, Progr. Nucl. Energy 29 (1995) 345.
[3] N. Nitani, T. Yamashita, T. Ohmichi, T. Muromura, in: Proc. 10th Pacific Basin Nucl. Conf. (10-PBNC), Kobe, Japan, 20–25 October 1996, vol. 2, Atomic Energy Soc. Japan, 1996, p. 1114.
[4] N. Nitani, H. Yokoi, T. Yamashita, T. Ohmichi, T. Matsui, T. Muromura, J. Nucl. Mater. 247 (1997) 59.
[5] T. Yamashita, H. Akie, H. Kimura, H. Takano, T. Muromura, IAEA-TCM, Victoria, Canada, 28 April–1 May 1998, to be published.
[6] T. Muromura, T. Yamashita, T. Ohmichi, H. Akie, H. Takano, in: Proceedings of the 14th Japan–Korea International Seminar on Ceramics, Kanazawa, Japan, 25–27 November 1997, p. 127.
[7] D.L. Hargman, MATPRO-Version11, A Handbook of Materials Properties for Use in the Analysis of Light Water Reactor Fuel Rod Behavior, Idaho National Eng. Lab, 1981.
[8] W.D. Kingery, H.K. Bowen, D.R. Uhlmann, Introduction to Ceramics, Wiley, New York, 1976.
[9] I. Barin, Thermochemical Data of Pure Substance, VCH, Weinheim, 1989.
[10] Y.S. Touloukian, R.W. Powell, C.Y. Ho, P.G. Klemens, Thermochemical Properties of Matter, vol. 2, Thermal conductivity, Non-metallic solids, IFI/Plenum, New York, 1970.
[11] J.C. Maxwell, A Treatise on Electricity and Magnetism 1 (1904) 441.
[12] T. Nishijima, T. Kawada, Nippon Genshiryoku Gakkaishi 6 (1964) 154.

[13] D. Dinos, D.L. Kohlstedt, J. Am. Ceram. Soc. 70 (1987) 531.
[14] M. Nauer, C. Carry, Scripta Metall. 24 (1990) 1459.
[15] H.J. Frost, M.F. Ashby, Deformation-Mechanism Maps, Pergamon, New York, 1982.